https://doi.org/10.1016/j.snb.2017.12.125

In situ μ-printed optical fiber-tip CO_2 sensor using a photocrosslinkable poly(ionic liquid)

Jushuai Wu[a], Ming-jie Yin[a], Karoline Täuber[b], Alessandro Dani[b], Ryan Guterman[b], Jiayin Yuan[b,1], A. Ping Zhang[a,*], and Hwa-Yaw Tam[a]

[a] *Photonics Research Center, Department of Electrical Engineering, The Hong Kong Polytechnic University, Hong Kong SAR, China*

[b] *Max Planck Institute of Colloids and Interfaces, Department of Colloid Chemistry, D-14424 Potsdam, Germany*

Abstract

Carbon dioxide (CO_2) sensors play important roles in our daily life and production activities. However, it remains a challenge to develop a tiny device with remote sensing capability for detection of CO_2 concentration and related parameters. Here we present an optical fiber-tip CO_2 sensor for simultaneous measurement of CO_2 concentration and temperature. A photocrosslinkable poly(ionic liquid), i.e. poly(1-allyl-3-vinylimidazolium bromide) (PAVB), with good CO_2 adsorption capability and selectivity was synthesized to fabricate miniature sensors via an in situ optical μ-printing technology. We directly printed several micrometer-scale Fabry–Pérot interferometers (FPIs) on the end face of a multicore optical fiber using the PAVB and SU-8 epoxy, respectively. We have demonstrated that the PAVB FPI sensor can measure CO_2 concentration with a sensitivity up to ~35 pm/% in the wide range of 0% – 75%, and its rise and fall dynamic response times are about 6.1 and 8.0 min, respectively. Meanwhile, the SU-8 FPI sensor is able to measure temperature with a sensitivity 0.059 nm/°C. Such a tiny CO_2 sensor can remotely and simultaneously measure CO_2 concentration and temperature in very small spaces and is thus promising for many applications ranging from waste gas detection to food quality control.

Keywords

Optical fiber sensor, carbon dioxide sensor, optical microfabrication, poly(ionic liquid)

[1] Present address: Department of Chemistry and Biomolecular Science, Center for Advanced Materials Processing, Clarkson University, 13699 Potsdam, NY, USA.

[*] Corresponding author. Tel.: +852 34003336; fax: +852 23301544; E-mail address: azhang@polyu.edu.hk (A. P. Zhang).

1. Introduction

Carbon dioxide (CO_2) is not only an essential gas for the proper functioning of the biosphere but also a common by-product of industrial activities. CO_2 sensors play crucial roles in agriculture and food control [1-3], industrial activities and air quality monitoring [2,4,5], and public healthcare [6,7]. For instance, CO_2 is not only one of the by-products of food spoilage but also a commonly used active gas for the reduction of the metabolic rates of microbes in food packaging applications [1,2]. Therein, CO_2 is an important and direct indicator of food quality; the development of accurate, reliable, fast-response, and non-destructive CO_2 sensors is highly demanded for active and intelligent food quality control.

CO_2 sensors can be generally classified into electrochemical and optical types according to their sensing mechanisms. Most of the currently prevailing CO_2 sensors, such as the potentiometric, amperometric, and conductometric sensors, are based on electrochemical principles [6]. Conventional potentiometric CO_2 sensors (e.g. Severinghaus CO_2 sensor) employ an indirect method of measurement [7], which monitors the change of pH value induced by the dissociation of CO_2 in electrolyte solutions. With the advent of microtechnologies, solid-state electrolyte sensors are rapidly replacing CO_2 sensors based on wet electrochemical processes. However, solid-state electrolyte sensors are commonly required to be locally heated at high temperature (300 ^oC–800 ^oC) to initiate chemical reactions [8-11], which results in long-term instability issues and limited scope of applications.

Optical CO_2 sensors are passive (i.e. do not require electricity power) and chemically inert, potentially allowing to overcome the drawbacks of electrochemical sensors for harsh environment (e.g. flammable or corrosive conditions) and/or remote sensing applications. Well-known optical CO_2 sensors include infrared detectors, which are based on light absorption in the infrared region [12,13]; colorimetric-type sensors, whose functioning is based on color change of pH indicator dye [14,15]; and fluorescent-type sensors, based on

fluorescence change of a luminescent dye [16-18]. However, most of these traditional CO_2 sensors are usually bulky and expensive. A promising solution to miniaturize optical CO_2 sensors is based on optical fiber technology. For instance, Munkholm *et al* demonstrated an optical fiber-tip CO_2 sensor obtained by depositing a polymer membrane with a pH sensitive fluorescent dye on the end surface of an optical fiber [19]; Segawa *et al.* fabricated a fiber-tip CO_2 sensor using a polymer film containing indicator dyes via dip-coating technology [20]. The main drawbacks of the dye-containing polymers are their low biocompatibility and long-term stability. Furthermore, the accuracy of these intensity-based optical sensors is generally not satisfactory due to light source instability.

In this paper, we propose a new fiber-optic CO_2 sensor fabricated via in situ optical printing of dye-free polymer Fabry–Pérot interferometers (FPIs) on the end face of an optical fiber. A photocrosslinkable poly(ionic liquid) (PIL), i.e. poly(1-allyl-3-vinylimidazolium bromide) (PAVB), with a large number of imidazolium functional groups was synthesized for reversible adsorption of CO_2 gas. Using an own-developed optical 3D μ-printing technology [21,22], we directly micropatterned the photocrosslinkable PAVB on the end face of optical fibers for sensor development. Several FPIs were fabricated on the end face of a multicore optical fiber using PAVB and commercial SU-8 epoxy resin, as shown in Fig. 1. Due to the different molecular structures of the two polymer materials, the PAVB FPI sensor can be used to selectively detect CO_2, while the SU-8 FPI sensor can serve as a reference temperature sensor. Such a small fiber-optic CO_2 sensor exhibited good performance in the simultaneous measurement of CO_2 concentration and temperature with good sensitivity and selectivity as well as a very wide dynamic operation range.

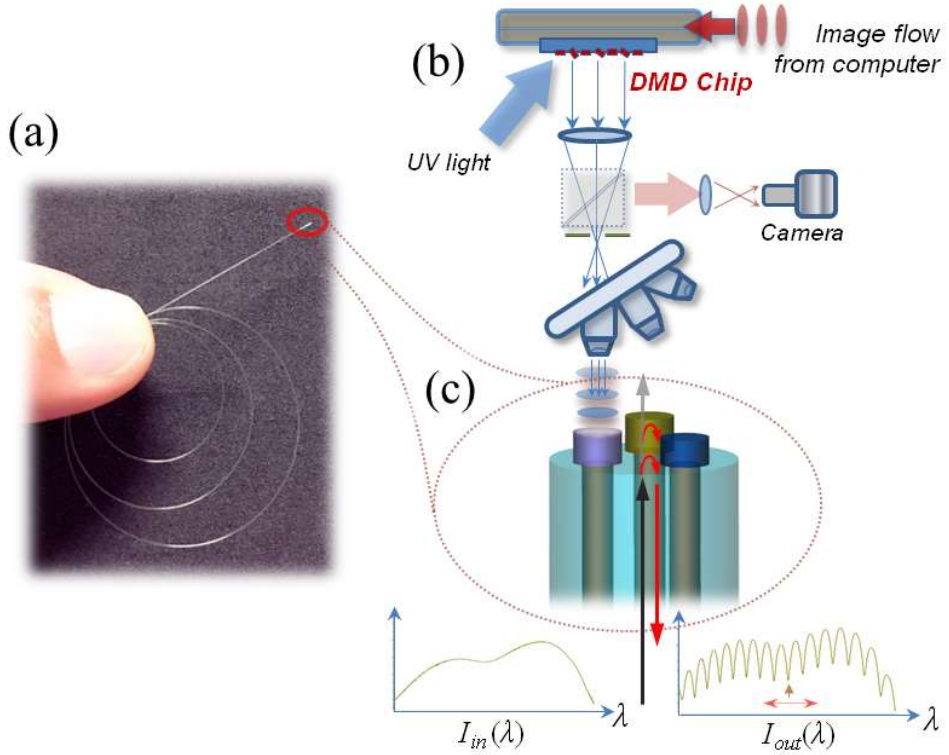

Fig. 1. Schematic illustration of the in situ printing of optical fiber-tip CO_2 sensors. (a) photograph of an optical fiber for sensor fabrication; (b) schematic of the optical μ-printing technology based on a digital-micromirror device (DMD); (c) schematic of the optical fiber-tip CO_2 sensor based on fiber-top Fabry–Pérot interferometers.

2. Material and Methods

2.1 Materials

All reagents were obtained from commercial suppliers and used without any further purification. 1-Vinylimidazole (99 %), 1-allyl bromide (98 %), 2,2'-azobis(2-methylpropionitrile) (98 %), 2-hydroxy-4'-(2-hydroxyethoxy)-2-methylpropiophenone (Irgacure 2959) were purchased from Sigma–Aldrich. EPON SU-8 resin was purchased from Momentive Limited. Tributylamine and octoxyphenylphenyliodonium hexafluoroantimonate were purchased form Meryer Chemical Technology (China) and Hampforford Research, respectively. Propyleneglycol monomethylether acetate and cyclopentanone were purchased from J&K Scientific (China). Dimethylsulfoxide, isopropanol (IPA) and ethanol (EtOH) were analytical grade. DI water with a resistance of 18 MΩ cm was used in all experiments.

2.2 Synthesis and characterization of the PAVB

It was demonstrated that PILs could reversibly capture and release CO_2 with high selectivity due to the interaction between the imidazolium cations and CO_2 molecules [23-28]. To enable the optical processing of PILs for device fabrication, we synthesized a photocrosslinkable PIL with imidazolium functional groups in two steps. As shown in Fig. S1, 1-vinylimidazole (monomer) and 2,2-azobisisobutyronitrile (initiator) were dissolved in the dimethylsulfoxide solvent and then polymerized at 90 ºC for 24 h to form poly(1-vinylimidazole). Thereafter, the polymer was further quaternized with 1-allyl bromide at 90 ºC to produce the photocrosslinkable PAVB.

The CO_2 adsorption property of the synthesized PAVB was characterized by the gas sorption method. The CO_2 adsorption experiments were conducted at 273 K using Quadrasorb and Autosorb 1-MP machines (Quantachrome Instruments). Isosteric heats of adsorption were calculated using the AS1Win software provided by Quantachrome Instruments. Before all adsorption experiments, the samples were degassed overnight at 363 K under dynamic vacuum. High purity gases were used for all measurements.

Fig. S2 shows the measured adsorption and desorption isotherms, collected through loading-unloading cycles with different maximum CO_2 pressures, i.e. 0.3, 0.6, 0.9, and 1.0 bar. One can see that the adsorption of CO_2 generally increases with the loading pressure. For maximum pressures of 0.3 and 0.6 bar, the adsorption and desorption isotherms depend almost linearly on the CO_2 pressure, and the corresponding maximum adsorptions are 1.14 and 2.15 cc g^{-1}, respectively. In both cases, hysteresis loops are observed, which indicate that the adsorption of CO_2 in PAVB results from both physisorption and chemisorption. For maximum pressures of 0.9 and 1.0 bar, the corresponding maximum adsorptions are 4.81 and 6.99 cc g^{-1}, respectively. At these pressures, the severity of the hysteresis effect becomes more

significant and the hysteresis loops remained open when the CO_2 pressure returned to zero (after a complete loading and unloading cycle). The results revealed that PAVB is a qualified functional polymer for the development of CO_2 sensors because of its good CO_2 adsorption properties.

2.3 Optical micropatterning of the PAVB

The PAVB and Irgacure 2959 (as photoinitiator) were dissolved in DI water for optical micropatterning. In 2D micropatterning experiments (including the sensor fabrication), the concentrations of the PAVB and Irgacure 2959 were 40 wt% and 3 wt%, respectively, whereas the concentrations of the PAVB and Irgacure 2959 were 30 wt% and 5 wt%, respectively, in 3D micropatterning experiments. The PAVB aqueous solution was dropped on a glass slide with a spacer, and then a cover glass was placed upon the solution. An optical 3D μ-printing platform based on a UV light source (at the wavelength of 365 nm) and a digital-mirror device (DMD, DLi4120 0.7" XGA, Texas Instruments), shown in Fig. 1(b), has been used to pattern the own-synthesized PAVB. The predesigned microstructures were converted into image data and then loaded onto the DMD chip for generation of optical patterns. UV light penetrated the cover glass and activated the crosslinking of the PAVB on the bottom side of the cover glass. The exposed micropatterns were developed by using EtOH.

Fig. 2 shows the images of the fabricated PAVB microstructures, which were taken by using a laser scanning confocal microscope (VK-X200, KEYENCE, Japan). Fig. 2(a) and Fig. 2(b) are the logos of the two collaboration units, i.e. The Hong Kong Polytechnic University (PolyU) and Max Planck Institute (MPI), respectively. The optimized exposure time was 10 s under a UV intensity of 96.89 mW cm^{-2}, and the development time was around 7 min in EtOH. It can be seen that the PAVB can be patterned into complex geometries with high resolution. With a specially designed testing pattern, the smallest feature size of PAVB microstructures was measured to be 5.5 μm, see Fig. S3. The PAVB can also be used to fabricate some

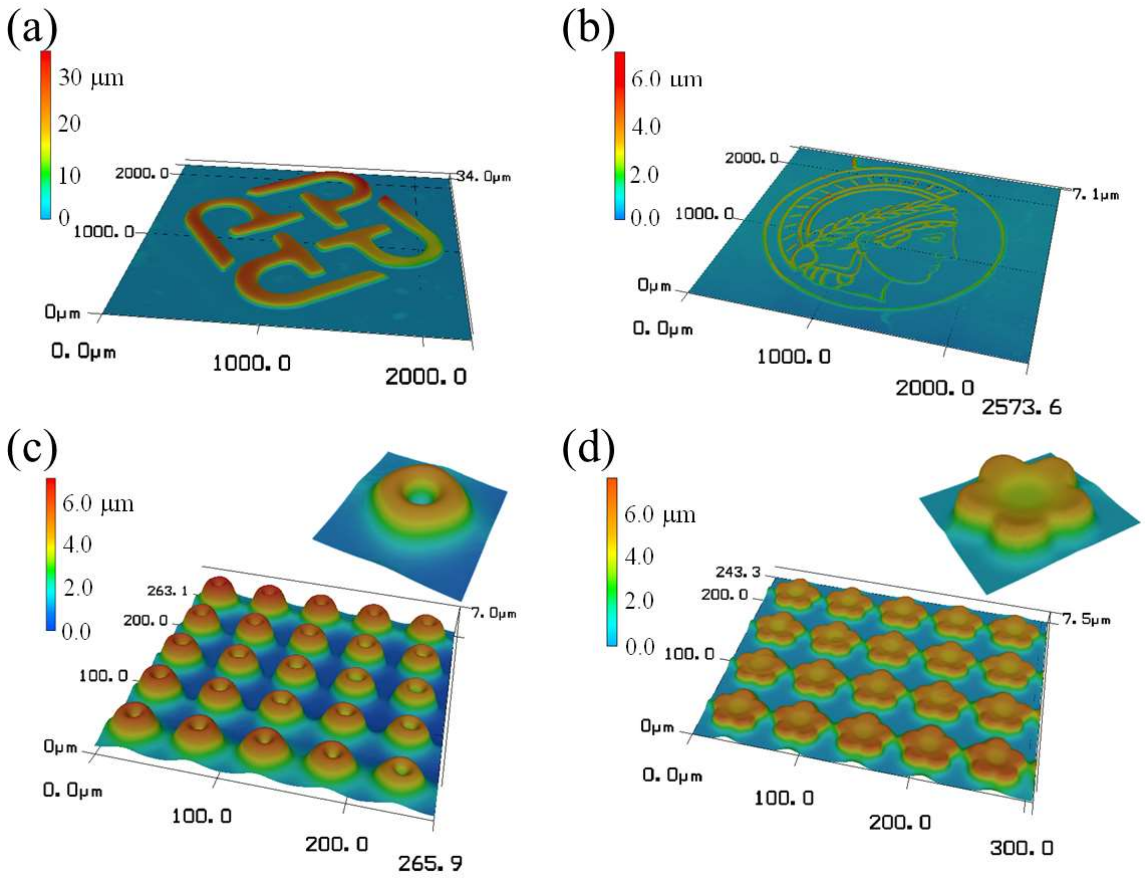

Fig. 2. Laser scanning confocal images of PAVB microstructures. (a) PolyU logo, (b) MPI logo, (c) micro-nozzle array, and (d) micro-flower array.

microstructures with 3D features. Fig. 2(c)-(d) show some fabricated PAVB micro-nozzle and micro-flower arrays, in which slice images of their 3D models have been used for a layer-by-layer optical exposure process. The total exposure time for these 3D micropatterns was around 30 s under a UV intensity of 160.33 mW cm^{-2}, slightly longer than the one used for 2D patterns. More details of the PAVB micro-flower structures are provided in Fig. S4.

To fabricate FPIs, PAVB films were deposited on the end faces of optical fibers by using a dip-coating method. The light intensity and total exposure time of the optical printing process were 96.89 mW cm^{-2} and 30 s, respectively.

2.4 Setup for testing the CO_2 sensor

A stainless steel cylinder gas chamber was used to seal the fiber-optic FPI CO_2 sensor, as shown in Fig. 3. The gas samples of different concentrations were prepared by mixing pure CO_2 gas with pure nitrogen at different flow rate ratios at atmospheric pressure through two

flow regulators. The sample gas flowed into the gas chamber at a constant speed in all the experiments. The light from a broadband source was coupled to and back from the seven-core optical fiber through a multicore fiber fan-in/out device. The reflection spectra of the fiber-optic sensors were measured by using an optical spectrum analyzer with a resolution of 0.02 nm.

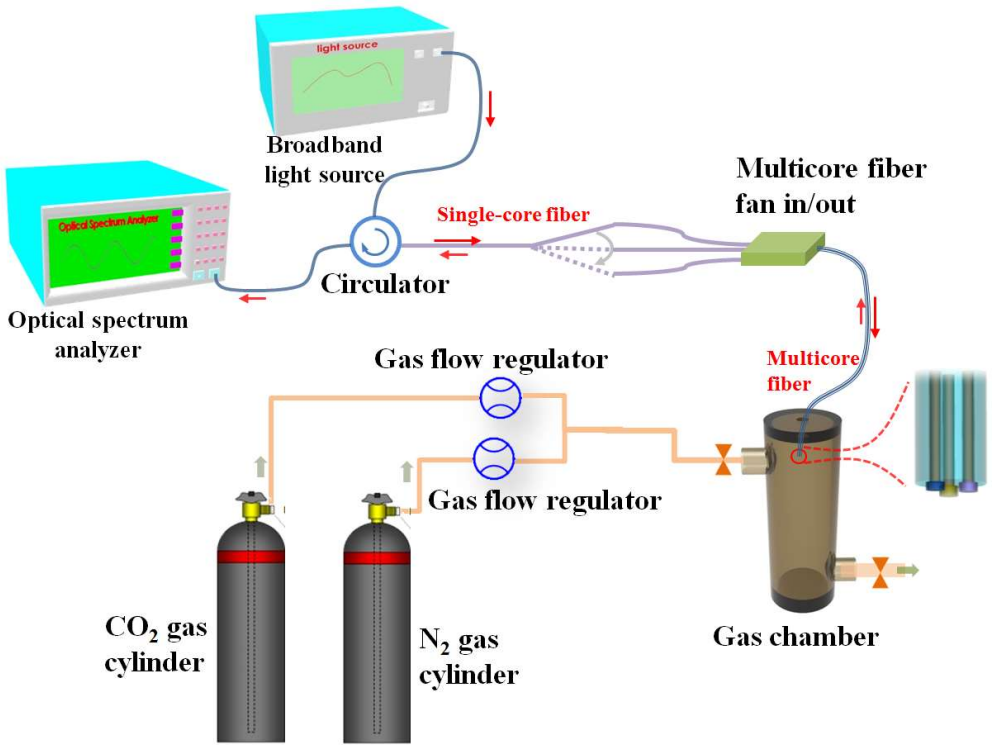

Fig. 3. The schematic of the experimental setup for the testing of the fiber-optic CO_2 sensor.

3. Results and Discussion

3.1 In situ printed optical fiber-top polymer FPIs

The good processability of the PAVB makes it possible to develop new functional microdevices and sensors. Since the optical fiber tip is a unique and tiny platform inherently coupled with light waves [29-33], we here in situ print PAVB on the end face of an optical fiber to develop miniature optical fiber-tip interferometer sensors. Fig. 4 shows two kinds of polymer FPI sensors fabricated on the end faces of single-core and multicore optical fibers.

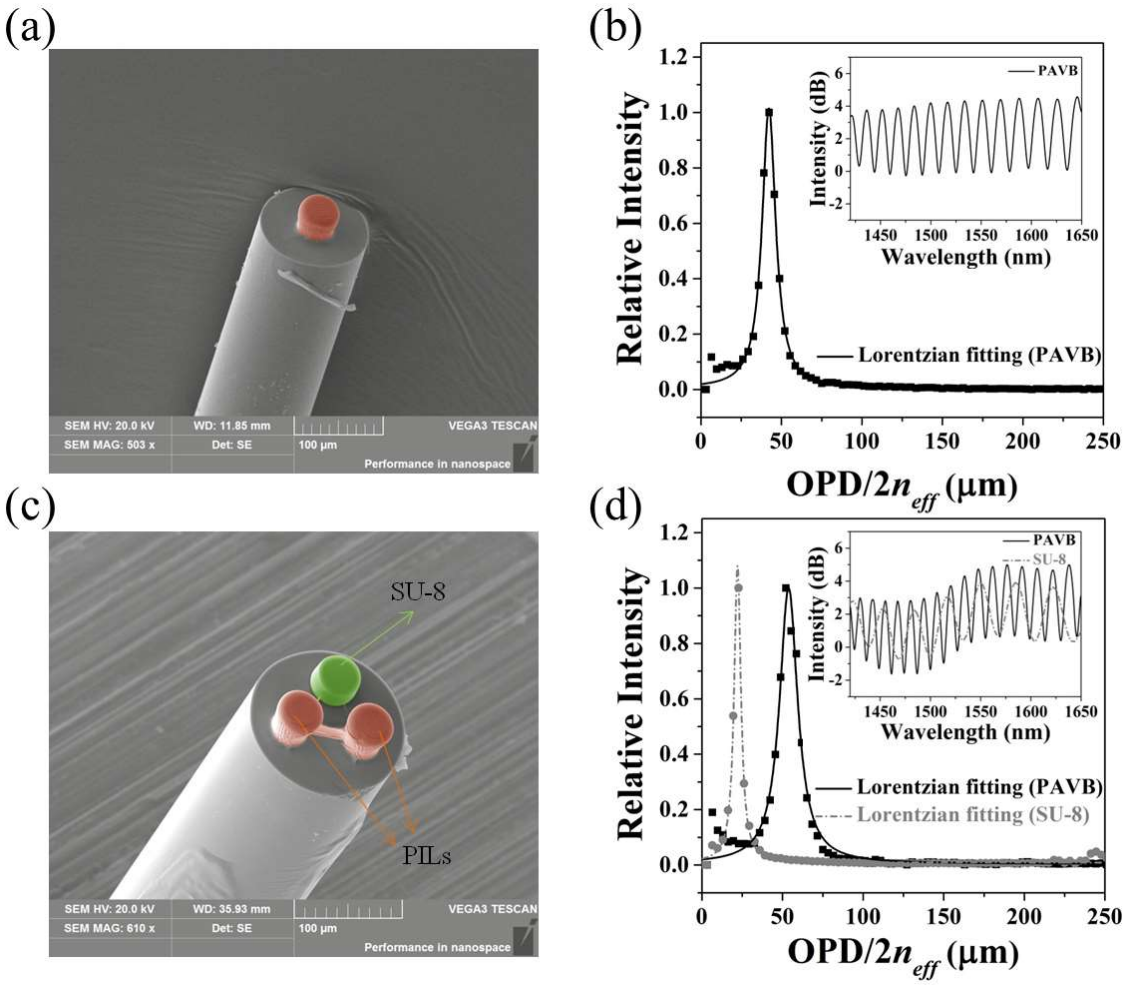

Fig. 4. SEM images and spectral characteristics of the fabricated optical fiber-top polymer FPIs. (a) SEM image of the PAVB FPI sensor fabricated on a standard single-core SMF. (b) Measured reflection spectrum (inset) and its corresponding FFT result. (c) SEM image of the PAVB and SU-8 FPI sensors fabricated on the end face of a multicore optical fiber. (d) Measured reflection spectrum (inset) and its corresponding FFT result.

Fig. 4(a) is a scanning electron microscopy (SEM) image of the PAVB FPI sensors fabricated on a standard single-core single-mode fiber, and Fig. 4(b) shows the measured reflection spectrum and its fast Fourier transformation (FFT) result. One can see that the top surface of the interferometer is smooth, which leads to good reflectivity of light. Therefore, the light waves reflected from the two interfaces, i.e. the interface between the glass and PAVB as well as that between the PAVB and surrounding gases, will interfere and form interference fringes in the output spectrum, as shown in the inset of Fig. 4(b). The free spectral range (FSR) of the interference fringe is 17.67 μm. The FFT results of the reflection spectrum reveal that the

length of the optical interferometer is 42.21 μm, which agrees very well with the values measured from the microscope image. In order to achieve a tiny fiber-optic CO_2 sensor, we fabricated three optical interferometer sensors on the end face of a multicore optical fiber for simultaneous detection of CO_2 and temperature. Fig. 4(c) shows the SEM images of fabricated tiny fiber-optic CO_2 sensors. The two longer interferometers were made from the PAVB, whereas the shorter one was made from commercial SU-8 epoxy resin. The material mixture ratio and fabrication conditions for the SU-8 FPI are the same as our previous work [21]. Since the spectra of the two PAVB interferometers are very close to each other, only one reflection spectrum of PAVB FPIs is presented in Fig. 4(d). The FSRs of the reflection spectra of the SU-8 and PAVB interferometers fabricated on the multicore optical fiber are 33.25 and 14.01 μm, and the corresponding lengths of the two interferometers are 22.08 and 53.78 μm, respectively.

3.2 Performances of the optical fiber-tip CO_2 sensors

It is known that the wavelength shift $\Delta\lambda$ of the interference reflection spectrum of a fiber-optic FPI is

$$\Delta\lambda = 4\pi\Delta(n_{eff}l)/\phi_b, \quad (1)$$

where $\Delta(n_{eff}\,l)$ and ϕ_b are the change of optical thickness and the phase bias of specific interference peak, respectively [34-37]. Therefore, any small change of the refractive index or the length of the FPI will induce a shift of the interference peak. When the FPI is made from PAVB, one can use the wavelength of the interference peak of the reflection spectrum to monitor the concentration of CO_2 as the adsorption of CO_2 will induce a change of the PAVB's refractive index.

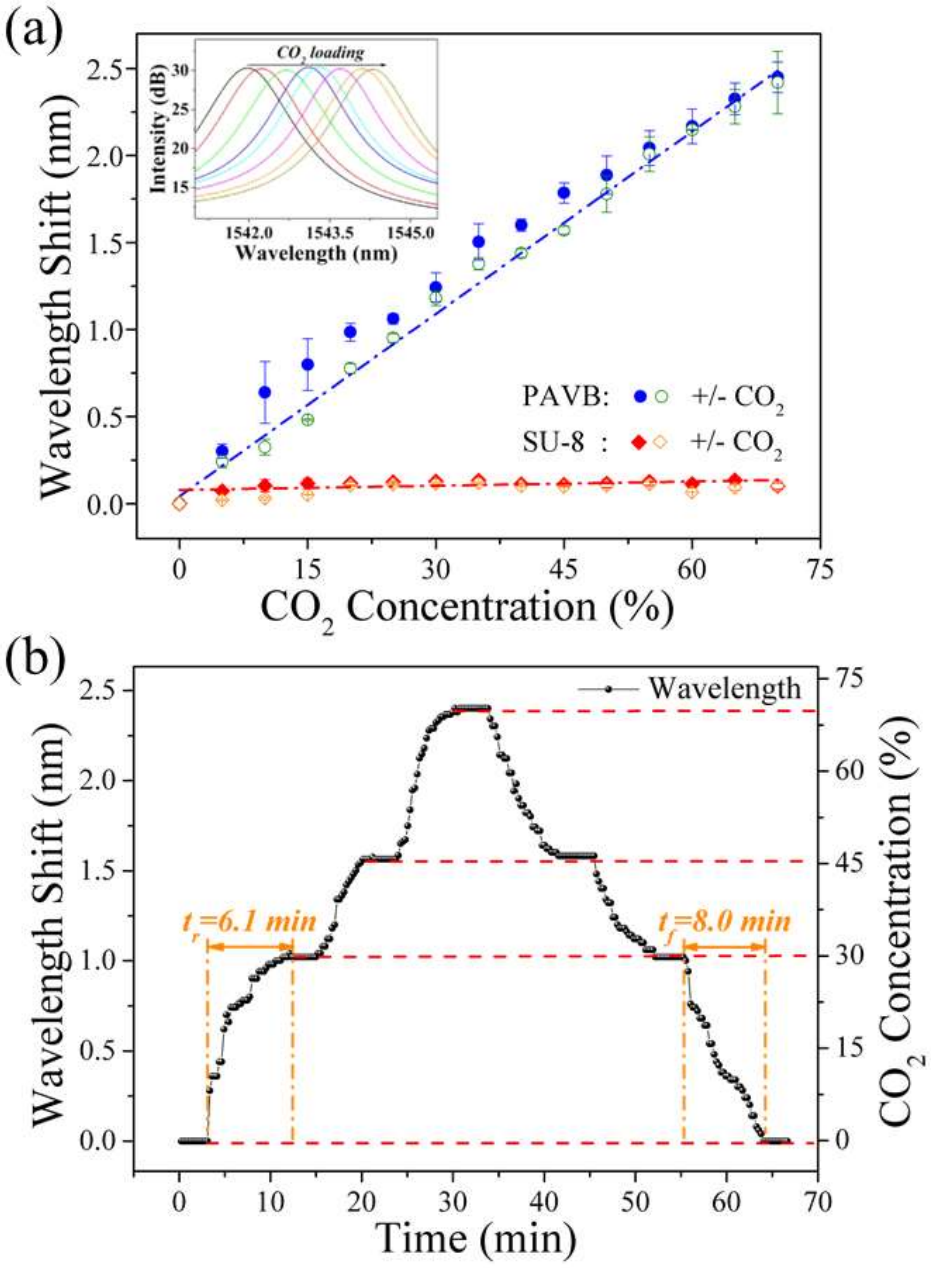

Fig. 5. Responses of the fabricated optical fiber-tip CO_2 sensor to the change of CO_2 concentration. (a) Reponses of the PAVB and SU-8 FPI sensors to the loading and unloading of CO_2 gas. The inset shows the shift of the spectral peak of the PAVB FPI sensor. (b) Dynamic response of the PAVB FPI sensor to the change of CO_2 concentration.

Fig. 5 shows the response of the optical fiber-tip sensor to the change of CO_2 concentration. Fig. 5(a) shows the responses of the PAVB and SU-8 FPI sensors to the loading and unloading of CO_2 gas at atmospheric pressure. One can see that the PAVB FPI sensor shows good linearity and reversibility when monitoring CO_2 concentrations ranging from 0 to 75%. The sensitivity of the sensor is 34.92 pm/%. In contrast, the SU-8 FPI sensor

shows zero responsivity to the change of CO_2 concentration due to the inertness of SU-8 when exposed to CO_2.

The dynamic response of the PAVB FPI sensor to the change of CO_2 concentration is shown in Fig. 5(b). The rise and fall times of the sensor's dynamic response are 6.1 and 8.0

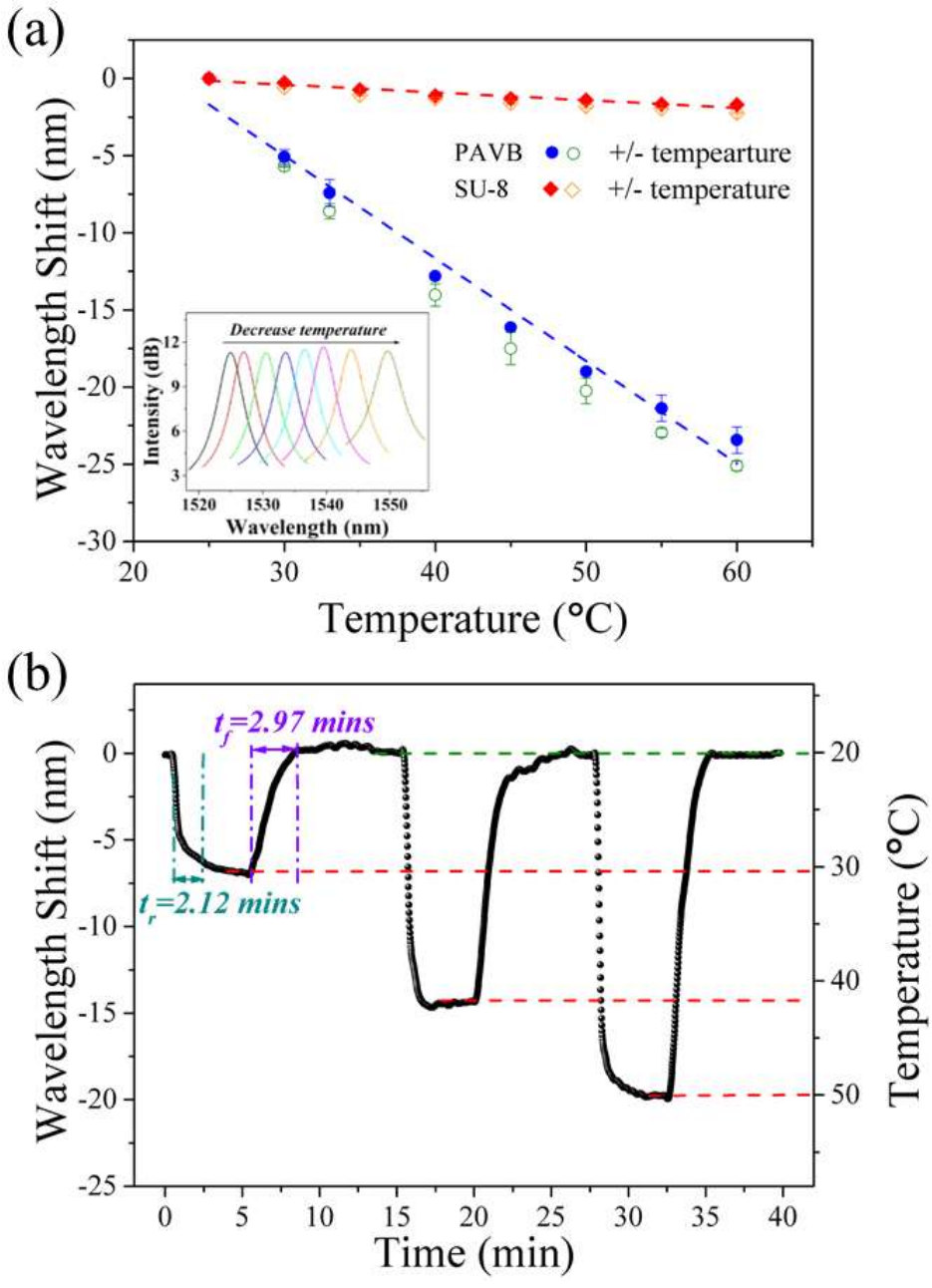

Fig. 6. Responses of the fabricated optical fiber-tip CO_2 sensor to the change temperature. (a) Responses of the PAVB and SU-8 FPI sensors to the change of temperature. The inset shows the shift of the spectral peak of the PAVB FPI sensor. (b) Dynamic response of the PAVB FPI sensor to the change of temperature.

min, respectively. Compared to other PIL-based CO_2 sensors [38,39], the response of this optical fiber-top PAVB FPI is much faster, which is attributed to the enhanced surface-area-to-volume ratio conferred by the microscale doming structure of the sensor.

Fig. 6 shows the responses of the PAVB and SU-8 FPI sensors to the change of environmental temperature. It can be seen that the increment of temperature results in a blue shift of the reflection spectra for both PAVB and SU-8 FPIs. In particular, the thermal sensitivity of PAVB FPI device is 0.704 nm/°C (as shown in Fig. 6(a)), which is much higher than that of SU-8 FPI, i.e. 0.059 nm/°C. The reason for such a significant difference is the higher mobility of PAVB chains compared to SU-8 chains at high temperature. Nevertheless, one can use the SU-8 FPI as a reference temperature sensor to eliminate the PAVB FPI's cross sensitivity to CO_2 concentration and temperature, as both polymer FPI sensors showed linear response to the change of temperature. The dynamic response of the PAVB FPI sensor to the change of temperature is shown in Fig. 6(b). The rise and fall times of the sensor are 2.12 and 2.95 min, respectively.

3.3 Discussion

Microengineering of functional polymeric materials has become a very appealing approach to develop new microdevices and sensors. In this work, we demonstrated an in situ optical µ-printing technology to process a photocrosslinkable PIL, i.e. PAVB, to fabricate a CO_2 sensor. It is known that CO_2 has much larger polarizability and quadrupole moment than other typical gases present in air, e.g. N_2 and O_2 [40]. As PAVB is an imidazolium-type polycation, CO_2 can be easily polarized in PAVB. Meanwhile, PAVB's cation groups and their sp^3 hybridizations can be readily rearranged into different configurations for CO_2 gas adsorption [41]. Moreover, the imidazolium rings in the main chain have a weak interaction with CO_2 gas [27]. All these interactions confer to PAVB a good CO_2 adsorption capacity and

selectivity. Moreover, compared to other polymers containing amino groups for CO_2 sensing [42,43], PAVB will not produce poisonous carbamates.

Although the detection limit of a fiber-optic sensor commonly depends on the overall performance of both the sensor and signal interrogation system, it is worth finding an approximate value of such a limit for comparison with other devices. If one assumes that a wavelength demodulation instrument with accuracy of 1 pm is used to interrogate the PAVB based optical fiber-tip FPI CO_2 sensor, one can use the sensitivity of 34.92 pm/% to obtain the estimated detection limit of the CO_2 sensor as 286 ppm. This value is comparable with the reported PIL-based CO_2 sensors [38], but lower than the one based on PIL-wrapped single-walled carbon nanotubes (SWCNTs), whose detection limit is 50 ppb [39]. However, the sensor based on PIL-wrapped SWCNTs can only be used in an oxygen-free environment and saturates at 50 ppm. In contrast, our optical fiber-tip CO_2 sensor has an extremely wide detection range, i.e. 0%–75%, which is highly demanded for many practical applications.

The optical fiber used in the fabrication of the fiber-tip CO_2 sensor is a seven-core optical fiber. Although we used only three cores of the optical fiber to fabricate two kinds of FPI sensors for simultaneous detection of CO_2 and temperature, the aforementioned strategy can be applied to integrate more kinds of functional polymers to detect a great number of parameters, such as humidity or other gas components. Its unique properties, such as very small size and multiparameter-sensing capability, make it very appealing for a large variety of applications, e.g. minimally invasive detection of food quality.

4. Conclusion

A photocrosslinkable PAVB has been synthesized to fabricate an optical fiber-tip CO_2 sensor via in situ optical μ-printing technology. With a multicore optical fiber, both the synthesized PAVB and commercial SU-8 epoxy resin have been directly printed on the end face of the

fiber to form a fiber-tip CO_2 sensor. Experimental results have revealed that the PAVB FPI sensor can rapidly detect the concentration of CO_2 gas in a very wide range of concentrations, from 0 to 75%, while the SU-8 FPI sensor is sensitive to the change of temperature only. Such a small CO_2 sensor is very promising for widespread applications ranging from industrial waste gas detection to food quality control.

Acknowledgements

This work was partially supported by Germany/ Hong Kong Joint Research Scheme (Grant No.: G-PolyU505/13), German Academic Exchange Service (DAAD, Grant No.: 57054931), and PolyU Strategic Development Special Project (Grant No.: 1-ZVGB).

Appendix A. Supplementary information

Supplementary information associated with this article can be found in the online version at xxx....

References

[1] S. Neethirajan, M.S. Freund, D.S. Jayas, C. Shafai, D.J. Thomson, N.D.G. White, Development of carbon dioxide (CO_2) sensor for grain quality monitoring, Biosyst. Eng., 106(2010) 395-404.

[2] S. Neethirajan, D.S. Jayas, S. Sadistap, Carbon Dioxide (CO_2) Sensors for the Agri-food Industry—A Review, Food Bioprocess Tech., 2(2008) 115-21.

[3] P. Puligundla, J. Jung, S. Ko, Carbon dioxide sensors for intelligent food packaging applications, Food Control, 25(2012) 328-33.

[4] I.P. de Vargas-Sansalvador, C. Fay, T. Phelan, M. Fernandez-Ramos, L. Capitan-Vallvey, D. Diamond, et al., A new light emitting diode–light emitting diode portable carbon dioxide gas sensor based on an interchangeable membrane system for industrial applications, Anal. Chim. Acta, 699(2011) 216-22.

[5] K. Kaneyasu, K. Otsuka, Y. Setoguchi, S. Sonoda, T. Nakahara, I. Aso, et al., A carbon dioxide gas sensor based on solid electrolyte for air quality control, Sens. Actuators, B, 66(2000) 56-8.

[6] K. Behera, S. Pandey, A. Kadyan, S. Pandey, Ionic Liquid-Based Optical and Electrochemical Carbon Dioxide Sensors, Sensors, 15(2015) 29813.

[7] J.W. Severinghaus, A.F. Bradley, Electrodes for blood pO2 and pCO_2 determination, J. Appl. Physiol., 13(1958) 515-20.

[8] T. Ishihara, K. Kometani, M. Hashida, Y. Takita, Application of mixed oxide capacitor to the selective carbon dioxide sensor I. Measurement of carbon dioxide sensing characteristics, J. Electrochem. Soc., 138(1991) 173-6.

[9] D.-D. Lee, S.-D. Choi, K.-W. Lee, Carbon dioxide sensor using NASICON prepared by the sol-gel method, Sens. Actuators, B, 25(1995) 607-9.

[10] G.G. Mandayo, F. González, I. Rivas, I. Ayerdi, J. Herrán, BaTiO3–CuO sputtered thin film for carbon dioxide detection, Sens. Actuators, B, 118(2006) 305-10.

[11] Q. Zhu, F. Qiu, Y. Quan, Y. Sun, S. Liu, Z. Zou, Solid-electrolyte NASICON thick film CO_2 sensor prepared on small-volume ceramic tube substrate, Mater. Chem. Phys., 91(2005) 338-42.

[12] J. Mulrooney, J. Clifford, C. Fitzpatrick, E. Lewis, Detection of carbon dioxide emissions from a diesel engine using a mid-infrared optical fibre based sensor, Sens. Actuators, A, 136(2007) 104-10.

[13] T. Yasuda, S. Yonemura, A. Tani, Comparison of the characteristics of small commercial NDIR CO_2 sensor models and development of a portable CO_2 measurement device, Sensors (Basel), 12(2012) 3641-55.

[14] C. von Bültzingslöwen, A.K. McEvoy, C. McDonagh, B.D. MacCraith, Lifetime-based optical sensor for high-level pCO_2 detection employing fluorescence resonance energy transfer, Anal. Chim. Acta, 480(2003) 275-83.

[15] S.M. Borisov, C. Krause, S. Arain, O.S. Wolfbeis, Composite Material for Simultaneous and Contactless Luminescent Sensing and Imaging of Oxygen and Carbon Dioxide, Adv. Mater., 18(2006) 1511-6.

[16] R.N. Dansby-Sparks, J. Jin, S.J. Mechery, U. Sampathkumaran, T.W. Owen, B.D. Yu, et al., Fluorescent-Dye-Doped Sol−Gel Sensor for Highly Sensitive Carbon Dioxide Gas Detection below Atmospheric Concentrations, Anal. Chem., 82(2010) 593-600.

[17] Z. Guo, N.R. Song, J.H. Moon, M. Kim, E.J. Jun, J. Choi, et al., A Benzobisimidazolium-Based Fluorescent and Colorimetric Chemosensor for CO_2, J. Am. Chem. Soc., 134(2012) 17846-9.

[18] Y. Liu, Y.H. Tang, N.N. Barashkov, I.S. Irgibaeva, J.W.Y. Lam, R.R. Hu, et al., Fluorescent Chemosensor for Detection and Quantitation of Carbon Dioxide Gas, J. Am. Chem. Soc., 132(2010) 13951-3.

[19] C. Munkholm, D.R. Walt, F.P. Milanovich, A fiber-optic sensor for CO_2 measurement, Talanta, 35(1988) 109-12.

[20] H. Segawa, E. Ohnishi, Y. Arai, K. Yoshida, Sensitivity of fiber-optic carbon dioxide sensors utilizing indicator dye, Sens. Actuators, B, 94(2003) 276-81.

[21] J. Wu, X. Guo, A.P. Zhang, H.Y. Tam, Rapid 3D micro-printing of polymer optical whispering-gallery mode resonators, Opt. Express, 23(2015) 29708-14.

[22] M.J. Yin, M. Yao, S.R. Gao, A.P. Zhang, H.Y. Tam, P.K.A. Wai, Rapid 3D Patterning of Poly(acrylic acid) Ionic Hydrogel for Miniature pH Sensors, Adv. Mater., 28(2016) 1394-9.

[23] J. Tang, H. Tang, W. Sun, H. Plancher, M. Radosz, Y. Shen, Poly(ionic liquid)s: a new material with enhanced and fast CO_2 absorption, Chem. Commun., (2005) 3325-7.

[24] J. Tang, H. Tang, W. Sun, M. Radosz, Y. Shen, Low-pressure CO_2 sorption in ammonium-based poly(ionic liquid)s, Polymer, 46(2005) 12460-7.

[25] P.G. Mineo, L. Livoti, M. Giannetto, A. Gulino, S. Lo Schiavo, P. Cardiano, Very fast CO_2 response and hydrophobic properties of novel poly(ionic liquid)s, J. Mater. Chem., 19(2009) 8861.

[26] J. Yuan, M. Antonietti, Poly(ionic liquid)s: Polymers expanding classical property profiles, Polymer, 52(2011) 1469-82.

[27] W. Fang, Z. Luo, J. Jiang, CO_2 capture in poly(ionic liquid) membranes: atomistic insight into the role of anions, Phys. Chem. Chem. Phys., 15(2013) 651-8.

[28] J. Yuan, D. Mecerreyes, M. Antonietti, Poly(ionic liquid)s: An update, Prog. Polym. Sci., 38(2013) 1009-36.

[29] G. Cojoc, C. Liberale, P. Candeloro, F. Gentile, G. Das, F. De Angelis, et al., Optical micro-structures fabricated on top of optical fibers by means of two-photon photopolymerization, Microelectron. Eng., 87(2010) 876-9.

[30] H.E. Williams, D.J. Freppon, S.M. Kuebler, R.C. Rumpf, M.A. Melino, Fabrication of three-dimensional micro-photonic structures on the tip of optical fibers using SU-8, Opt. Express, 19(2011) 22910-22.

[31] G. Kostovski, P.R. Stoddart, A. Mitchell, The Optical Fiber Tip: An Inherently Light‐Coupled Microscopic Platform for Micro‐and Nanotechnologies, Adv. Mater., 26(2014) 3798-820.

[32] T. Gissibl, S. Thiele, A. Herkommer, H. Giessen, Sub-micrometre accurate free-form optics by three-dimensional printing on single-mode fibres, Nat. commun., 7(2016).

[33] M. Vanek, J. Vanis, Y. Baravets, F. Todorov, J. Ctyroky, P. Honzatko, High-power fiber laser with a polarizing diffraction grating milled on the facet of an optical fiber, Opt. Express, 24(2016) 30225-33.

[34] P. Morris, A. Hurrell, A. Shaw, E. Zhang, P. Beard, A Fabry-Perot fiber-optic ultrasonic hydrophone for the simultaneous measurement of temperature and acoustic pressure, J. Acoust. Soc. Am., 125(2009) 3611-22.

[35] G.C. Hill, R. Melamud, F.E. Declercq, A.A. Davenport, I.H. Chan, P.G. Hartwell, et al., SU-8 MEMS Fabry-Perot pressure sensor, Sens. Actuators, A, 138(2007) 52-62.

[36] A. Sun, X.G. Qiao, Z.A. Jia, M. Li, D.Z. Zhao, Study of simultaneous measurement of temperature and pressure using double fiber Bragg gratings with polymer package, Opt. Eng., 44(2005).

[37] W.P. Chen, D.N. Wang, B. Xu, C.L. Zhao, H.F. Chen, Multimode fiber tip Fabry-Perot cavity for highly sensitive pressure measurement, Sci. Rep., 7(2017).

[38] C. Willa, J. Yuan, M. Niederberger, D. Koziej, When Nanoparticles Meet Poly(Ionic Liquid)s: Chemoresistive CO_2 Sensing at Room Temperature, Adv. Funct. Mater., 25(2015) 2537-42.

[39] Y. Li, G. Li, X. Wang, Z. Zhu, H. Ma, T. Zhang, et al., Poly(ionic liquid)-wrapped single-walled carbon nanotubes for sub-ppb detection of CO_2, Chem. Commun., 48(2012) 8222-4.

[40] J.L. Anthony, J.L. Anderson, E.J. Maginn, J.F. Brennecke, Anion effects on gas solubility in ionic liquids, J. Phys. Chem. B, 109(2005) 6366-74.

[41] S. Supasitmongkol, P. Styring, High CO_2 solubility in ionic liquids and a tetraalkylammonium-based poly (ionic liquid), Energy Environ. Sci., 3(2010) 1961-72.

[42] T.C. Doan, J. Baggerman, R. Ramaneti, H.D. Tong, A.T. Marcelis, C.J. van Rijn, Carbon dioxide detection with polyethylenimine blended with polyelectrolytes, Sens. Actuators, B, 201(2014) 452-9.

[43] T.C. Doan, R. Ramaneti, J. Baggerman, J.F. van der Bent, A.T. Marcelis, H.D. Tong, et al., Carbon dioxide sensing with sulfonated polyaniline, Sens. Actuators, B, 168(2012) 123-30.

Title: In situ μ-printed optical fiber-tip CO_2 sensor using a photocrosslinkable poly(ionic liquid)

Authors: Jushuai Wu[a], Ming-jie Yin[a], Karoline Seefeldt[b], Alessandro Dani[b], Ryan Guterman[b], Jiayin Yuan[b,1], A. Ping Zhang[a,*], and Hwa-Yaw Tam[a]

[a] Photonics Research Center, Department of Electrical Engineering, The Hong Kong Polytechnic University, Kowloon, Hong Kong SAR, China

[b] Max Planck Institute of Colloids and Interfaces, Department of Colloid Chemistry, D-14424 Potsdam, Germany

*E-mail: azhang@polyu.edu.hk

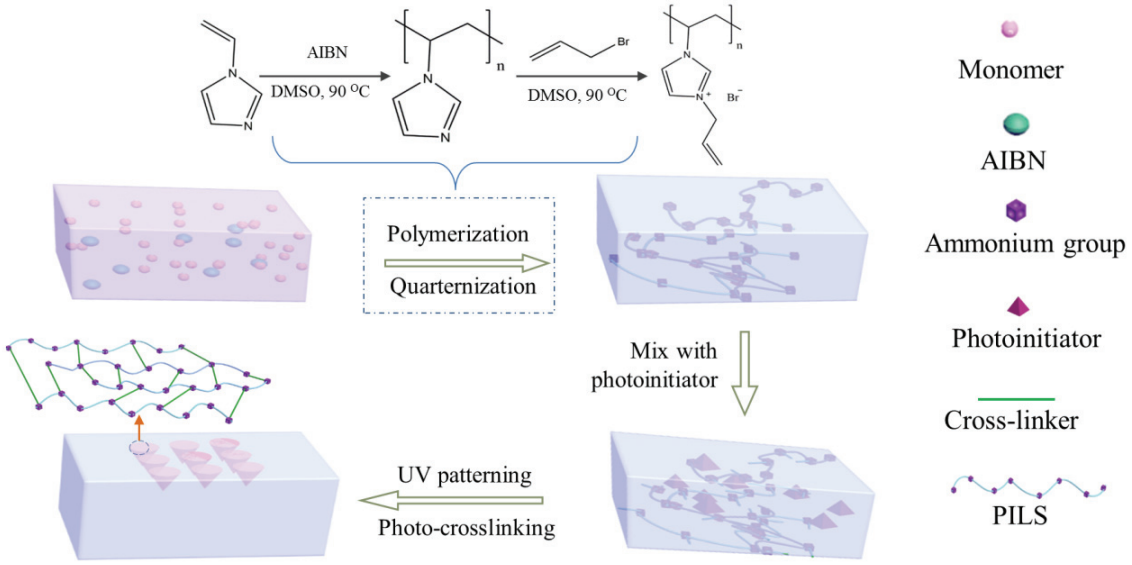

Figure S1. Schematic of the synthesis and photo-crosslinking processes of the poly(1-allyl-3-vinylimidazolium bromide) (PAVB).

[1] Present address: Department of Chemistry and Biomolecular Science, Center for Advanced Materials Processing, Clarkson University, 13699 Potsdam, NY, USA.

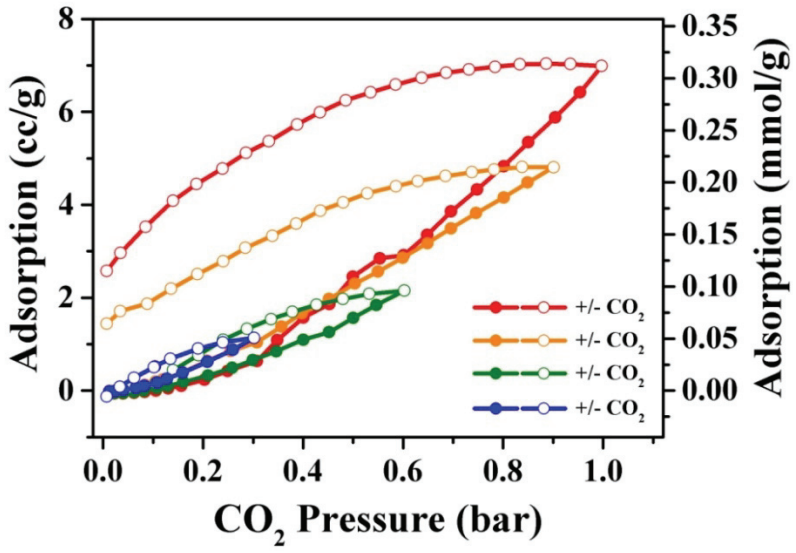

Figure S2. Adsorption and desorption isotherms of the PAVB. The measurements were repeatedly conducted under CO_2 pressures up to 0.3, 0.6, 0.9 and 1.0 bar, respectively.

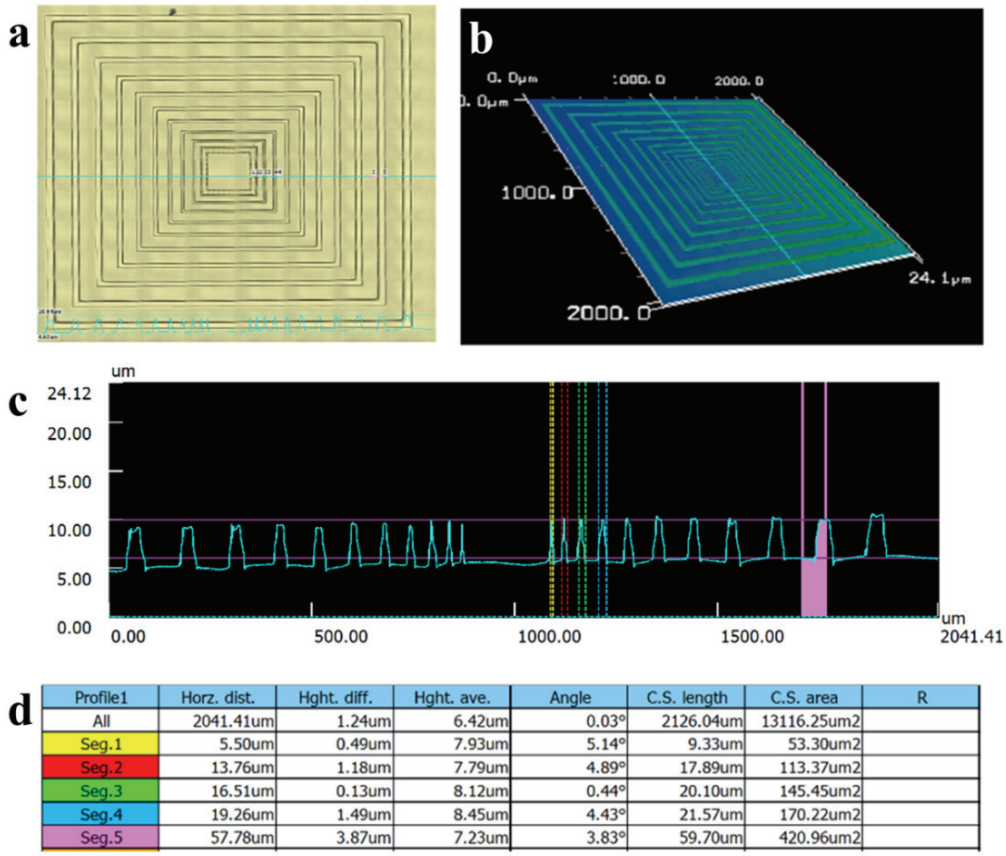

Profile1	Horz. dist.	Hght. diff.	Hght. ave.	Angle	C.S. length	C.S. area	R
All	2041.41um	1.24um	6.42um	0.03°	2126.04um	13116.25um2	
Seg.1	5.50um	0.49um	7.93um	5.14°	9.33um	53.30um2	
Seg.2	13.76um	1.18um	7.79um	4.89°	17.89um	113.37um2	
Seg.3	16.51um	0.13um	8.12um	0.44°	20.10um	145.45um2	
Seg.4	19.26um	1.49um	8.45um	4.43°	21.57um	170.22um2	
Seg.5	57.78um	3.87um	7.23um	3.83°	59.70um	420.96um2	

Figure S3. Laser scanning confocal image and its profile parameters of the fabricated concentric PAVB micro-squares.

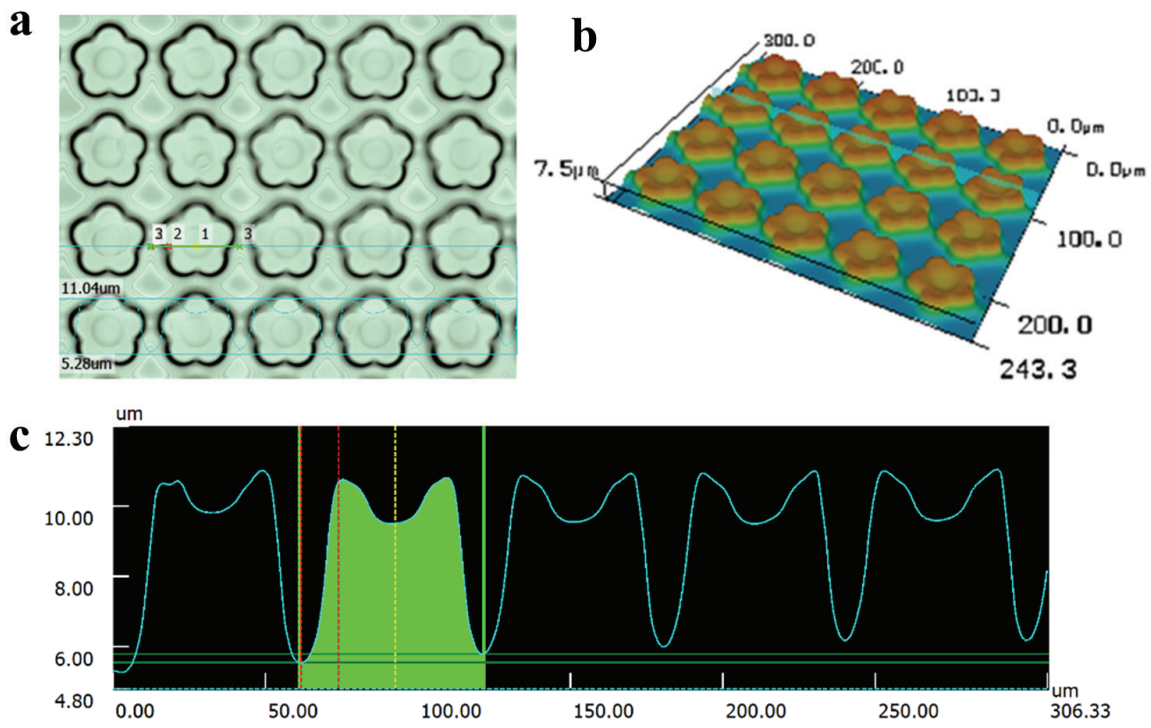

d

Profile1	Horz. dist.	Hght. diff.	Hght. ave.	Angle	C.S. length	C.S. area	R
All	306.33um	2.86um	9.21um	0.53°	322.10um	1354.26um2	
Seg.1	31.38um	3.96um	8.93um	7.19°	32.91um	132.25um2	
Seg.2	12.39um	5.12um	7.40um	22.48°	13.84um	32.90um2	
Seg.3	60.28um	0.24um	9.08um	0.23°	63.39um	259.99um2	

Figure S4. Laser scanning confocal image and its profile parameters of the fabricated PAVB microflower array.